Astron. Astrophys. 324, 1046–1058 (1997)

ASTRONOMY
AND
ASTROPHYSICS

Radiative shocks in atomic and molecular stellar-like atmospheres

VIII. A self-consistent comprehensive model

E. Huguet and J.-P.J. Lafon

Observatoire de Paris, DASGAL/UMR 335 C.N.R.S., F-92195 Meudon Cedex, France

Received 7 June 1996 / Accepted 7 October 1996

Abstract. This paper is devoted to the modelling of radiative shock waves propagating through a stellar-like atmosphere; that is a collisional atomic and molecular hydrogen gas with temperature and density ranges $1000\,K < T < 5000\,K$, and $10^{-14}\,g.cm^{-3} < \rho < 10^{-8}\,g.cm^{-3}$. Such ambient conditions are typical of those found in inner circumstellar envelopes of cool pulsating evolved stars.

The model describes a one dimensional steady-state radiative shock wave. The radiative coupling between the precursor (pre-shocked gas) and the wake (post-shocked gas) is fully self-consistent. It takes into account three radiations: the Lyman-α line, the Lyman continuum and the Balmer continuum, without any ETL assumption.

The wake is described up to the region in which the Balmer continuum flux is produced at about $100\,km$ behind the shock front.

Although the present paper completes the previous Papers of this series we write it as self-contained as possible in order to give a concise but global view of our investigations on radiative shock waves.

Key words: hydrodynamics – radiative transfer – shock waves – circumstellar matter – stars: mass loss – stars: AGB, post-AGB

1. Introduction

Strong radiative hypersonic shock waves can propagate in collisional media. This is an important phenomenon involved in processes starting mass loss in the inner layers of circumstellar envelopes of evolved stars: models of mass loss and mass loss rates are very sensitive to input physics, with significant consequences on star evolution tracks in the HR diagram (Lafon and Berruyer, 1991; Lafon, 1995). This is the reason why many attempts were made to obtain accurate physical descriptions. However, this is a very difficult problem because, in such shock structures, the fluids are strongly out of equilibrium and radiations introduces non local features and self-consistent coupling absent in collisional simply supersonic waves.

A non exhaustive list of the main specific difficulties related to the modelization of such shock waves includes at least the following set which must be taken into account.

First, a radiative precursor is generated by photons produced by recombinations beyond the front and this alters the whole structure of the shock. Now, this structure depends critically on all photons produced in the wake, but conversely the whole wake depends on photons eventually produced throughout the precursor. Such a coupling phenomenon is extremely difficult to handle because it is non local. The gas "chemistry", including changes of excitation levels and ionization is no longer a local phenomenon in which local balance equations could be written. Through photons the whole shock wave governs its structure at each point.

This induces a second fundamental problem: defining boundary conditions for models. In fact the actual boundaries are at infinity on both sides of the shock front for all phenomena, whereas model boundary conditions must be placed at finite distances, but in practice different for various phenomena. Thus, modelization requires the solution of self consistent stiff problem with consistent conditions on consistently moving boundaries.

A third problem is that modelling shocks over large size scales requires an accurate description of several microscopic processes unfortunately quantitavely and/or qualitatively badly known under the physical conditions which are effectively those in which they are at work, or under the approximations of the model. An instance is given by three-body recombinations which play a role in the radiative relaxation regions of the wake.

Finally, another problem is concerned with what happens through the hydrodynamical discontinuity, which is the smallest substructure. Collisions are more or less efficient compared to other phenomena and this produces significant effects beyond the front.

These few examples illustrate well the difficulty of the question. Fortunately, for shocks propagating in hydrogen, which is the major component of most of circumstellar envelopes of

Send offprint requests to: E. Huguet

evolved stars, it could be emphasized that, at least for steady state shocks, superposed more or less independant structures can exist simultaneously. Roughly speaking, the various physical processes are efficient at very different scales, which allows to distinguish different zones. Each zone is dominated by a small number of processes for which modelling is possible (Gillet and Lafon 1983, hereafter referred to as Paper I); for instance usual Rankine-Hugoniot jump relation govern the hydrodynamic discontinuity, at least for two different fluids ("heavy particles" and electrons). Now, a core structure surrounding the discontinuity is governed by the Lyman continuum radiation (Gillet and Lafon 1984; Gillet et al. 1989, hereafter respectively referred to as Papers II and III). A two level hydrogen atom is sufficient to describe the structure in a realistic way. However modelling a thick zone including the previous one requires a more complete model for the hydrogen atom. Note that, in spite of what could be imagined *a priori*, the aforementioned non local stiffness of the equations lead to difficulties even with a small number of energy levels in the hydrogen atom.

A very useful tool for solving such problems is the mean photon concept (Paper III): it allows to concentrate the energy of all the photons of one frequency band in one mean frequency which can be related, for free-bound radiations, to a mean temperature of the region which emit the radiation. This mean photon approximation allowed to progressively increase the size of the modelled structure step by step: adding a mean photon in the model requires describing those parts of the stucture in which the corresponding radiation is produced. Nevertheless, such extentions of the model are limited. In fact, each mean photon correspond to an atomic transition; consequently adding a mean photon to the model requires to take into account one more level in the hydrogen atom and so to take into account all the associated bound-bound transitions. This implies the treatment of transfer for lines for which the description in terms of a unique mean frequency may be too crude if diffusion is present (the mean photon approximation does not account for the lines shape). Nevertheless, for a three-level atom, a specific approximation linked to the very small lifetime of the first excited level of the hydrogen atom could be found (ZED approximation, see Huguet et al. 1994, hereafter referred to as Papers VI and VII respectively).

Finally, we recently were able to build a completely self-consistent model based on three mean photons. This allows to build the thickest self consistent two-fluid model now available and presented hereafter. Apart from its intrinsic interest it illustrates fairly well the above mentioned problems and enables to discuss with much more details the drawbacks or the limits of validity of available models and the strength of the constraints imposed by good input physics in future models.

Sect. 2. summarizes the hypotheses and approximations of the model. Sect. 3. is concerned by the numerical methods. Initial values and parameters are given in Sect. 4. The self-consistent model is analysed in Sect. 5. (general features of the shock wave structure) and Sect. 6. (detailed analysis). The consistency of the various approximations is analysed in Sect. 7. We conclude in Sect. 8. The microscopic reactions taken into account are listed in Appendix A. The equations of the model are listed in Appendix B. Non standard notation are defined in Appendix C.

2. Basic model assumptions

The model was described in Papers VI and VII. In this section we only summarize the main features of this model, including approximations with their range of validity. The microscopic processes taken into account and the equations used are given in appendices A and B respectively. Details can be found in Papers VI and VII.

2.1. General assumptions and approximations

1.) The flow is assumed mono-dimensional and in steady state.
2.) Conductivity, viscosity, diffusion, turbulence, magnetic fields and gravity are ignored.
3.) The velocity distribution is assumed maxwellian for particles of any species.
4.) The gas is composed of H_2-molecules, which can be dissociated, H-atoms which can be excited (only in the first level) or ionized. Gases of all species are perfect.
5.) Three radiations are taken into account: the Balmer and the Lyman continua and the Lyman-α line. The corresponding spectrum is reduced to a set of three "mean photons": in each part of the spectrum, the various frequencies are replaced by a unique mean frequency determined in such a way that the energy and the number of photons are conserved (Paper III, Appendix A).
6.) In the framework of the "mean-photon" approximation the absorption cross-section is defined as a mean value which can be only estimated. This difficulty has been discussed in Paper VI. Thereafter, we keep the same approximation *i.e.*, we take $\sigma_{12} = 10^{-13}\, cm^2$ for the photo-excitation cross section of the H-atoms by the Lyman-α photons.

2.2. Approximations concerning the precursor

The main problem in the precursor (as in the wake) is the radiative transfer. It is largely simplified when emission can be neglected in the precursor, which is the case when the shock is weak enough. "Weak enough" shocks are those for which:
1.) the ionization degree ($\alpha = n_{e^-}/n$) is small enough for free-bound transitions to be negligible (in the precursor); under typical shock conditions α must be smaller than about 0.1 (see Paper I).
2.) these are no excited atoms in the precursor except those produced by photo-excitation due to photons coming from the wake. This implies that the parameter $\tilde{T}_{e,L}$, which fixes the value of the Lyman continuum mean-photon ν_L, lies below about 12000 K. In such cases, the effects of the Lyman-α photons coming from the wake can be estimated using some specific approximation called "ZED" approximation, detailed in Paper VI.

For weak enough shocks, the two-point boundary value problem of the precursor can be reduced to an initial-value problem (Papers I and II) for the Lyman continuum. The Balmer continuum is optically thin.

It is also assumed that there are no interactions between molecules and Lyman-α photons, in spite of uncertainties concerning validity.

2.3. Approximations concerning the wake

After crossing the shock front the gas enters the wake. This complex relaxation zone was described qualitatively in Paper I. The description of the wake shows two main difficulties: the radiative transfer and the three-body recombinations. We summarize hereafter these problems and the methods used in previous Papers.

2.3.1. Radiative transfer

The problem comes from the existence of transition regions from an optically thin to an optically thick medium, for different radiations at different places. In extreme regions, the concerned radiations reach local equilibrium values which can be taken as boundary conditions for the corresponding transfer equations. This would not be a problem if the location of such regions, and some informations concerning the relative number densities (thereon RNDs; see definition in appendix C) or the thermodynamic variables, could be known *a priori*. In such a case the transfer equation, for each radiation, would be solved with some relaxation methods, and the complexity of the problem would be reduced to the self-consistent coupling of the wake with the precursor. Unfortunately, since the wake is far from equilibrium, the location of the aforementioned regions is determined by the relaxation times of the various physical processes. Consequently, the dominant phenomena are not well identified at each given distance before the complete solution is known. The same is true concerning the coupling between them. In such a context the prediction, with a sufficient accuracy, of the location of a region where the medium becomes optically thick for some radiation is a part of the whole problem. Thus, the difficulty in our transfer problem comes from the difficulty to know where the corresponding boundary conditions apply.

In our model we use a half-moment method (see Sherman 1968, and Paper III), in which the classical (steady state) transfer equation, without scattering, is splitted into two first order equations. In a frame linked to the shock front, the first half-moment corresponds to the flux propagating upstream ($x < 0$), the other corresponds to the flux propagating downstream ($x > 0$). The so-called net radiative flux is the sum of these two fluxes. Thus, the two-point boundary value problem is reduced to an initial-value problem (one initial value for each flux). In the framework of our "mean-photon" approximation, there are two equations for each continuum radiation (Balmer and Lyman) and one for the Lyman-α radiation, for which there is no net radiative flux because of the very short lifetime of the first excited level of the H-atom (see Papers VI and VII).

2.3.2. The three-body recombinations in the wake

There is a particular problem concerning the microscopic processes in the wake: some of them have never been studied under so "exotic" conditions. This is the case for the three-body recombinations.

As explained in Paper VII, a full treatment of this important process is a huge work. In particular, it requires a multi-level description of the H-atom. At the present time, such a description is incompatible with our "mean photon" approximation. However, a reliable estimation of the three-body recombination rate could be obtained in Paper VII: to summarize, we have extrapolated, in our range of parameters, an approximation due to Hinnov and Hirschberg (1962) by using the results of computations carried out by Bates et al. (1962). This approximation is expected to give at least the correct order of magnitude of the three-body recombination rate in the range of temperature and density of the wake. In any case, it enables us to get information about the role played by the three-body recombination process in radiative shock waves.

It is worth noting that the accuracy of our approximation probably increases with the distance from the shock front since the ambient conditions get closer to the range of validity of the initial approximation of Hinnov and Hirschberg.

3. The numerical method

The numerical method used was described in Papers VI and VII. Some improvements have been introduced concerning the wake: in particular we now use a Gear method for the computation of the one fluid region. This numerical scheme is faster than the Runge-Kutta's scheme used before, and the CPU-time is significantly reduced. Moreover, the Gear scheme is more convenient for the stiff problems and then more relevant for the integration of the transfer equations.

In any case, the instabilities appearing in the recombination regions make the branching to assymptotic solutions, in the two stream model, very difficult.

4. The new model: general features

As a new step of our progressive investigation started in 1983, we now can display a solution including in a self-consistent structure all regions from the radiative precursor to the Balmer recombination zone in a model without assumption of thermal equilibrium or ETL. Let us stress on the salient features of this model:

1) This is the first self-consistent model of a radiative shock wave including three radiations, the precursor and the wake. Our solution gives the structure of the wake up to the Balmer continuum recombination zone.

2) There is a steep velocity gradient (and so a high compression ratio) in the wake near the shock front.

3) It provides an estimate of the radiative loss (due to the Balmer continuum radiation) as 75% of the kinetic energy flux.

4) It suggests strongly that a radiative shock wave cannot

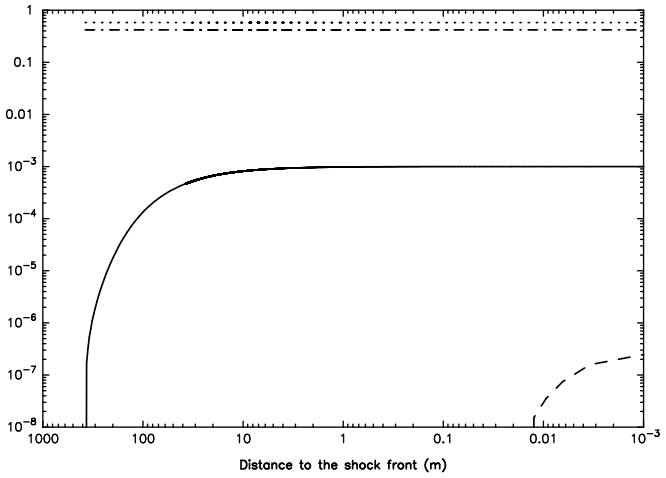

Fig. 1. RNDs versus distance from the shock front in the precursor, α (solid curve), β (dashed curve), δ (dotted curve) and ϵ (dashed-dotted curve).

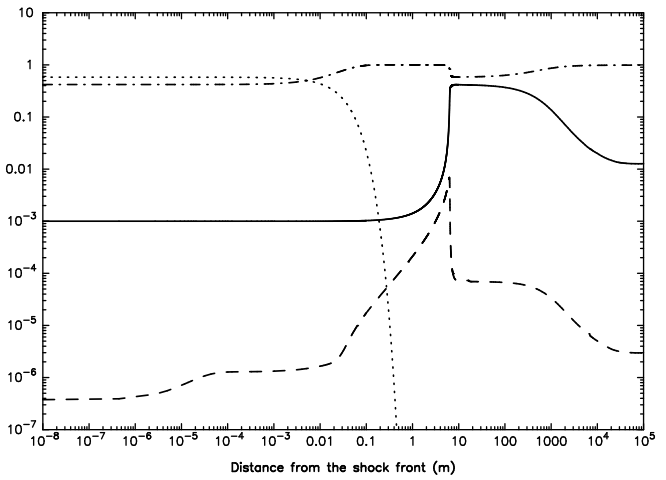

Fig. 2. RNDs versus distance from the shock front in the wake, α (solid curve), β (dashed curve), δ (dotted curve) and ϵ (dashed-dotted curve).

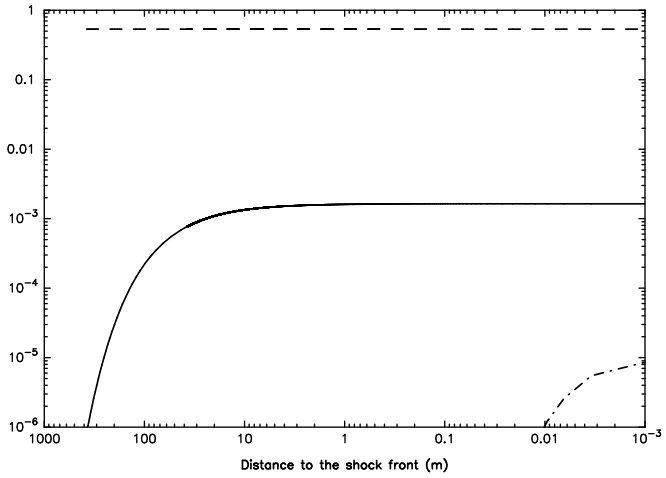

Fig. 3. Radiative fluxes versus distance from the shock front, in units of F_n (defined in Appendix C), in the precursor, Balmer continuum (dashed curve), Lyman continum (solid curve) and Lyman-α (dashed-dotted curve).

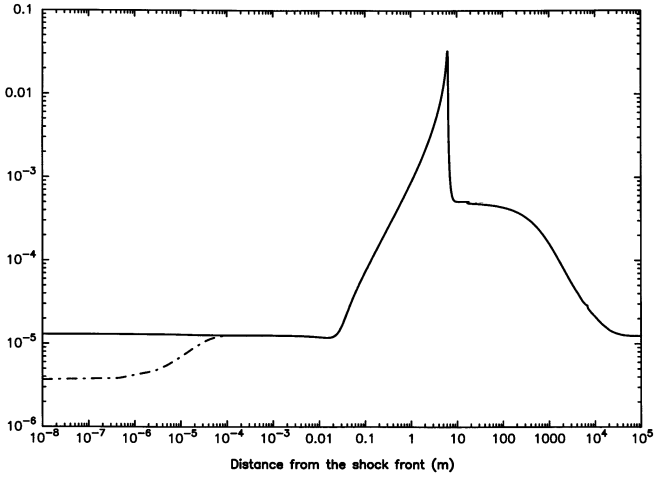

Fig. 4. a Lyman-α flux versus distance from the shock front (wake). F_α/F_n (solid curve), F_0^α/F_n (dashed-dotted curve).

cross the medium in which it propagates without perturbing it strongly.

The results of our computations are displayed Figs. 1 to 5.

The evolution of the RNDs through the radiative shock wave (Figs. 1 and 2) gives a good idea of its structure, in particular Figs. 1 and 2 show various regions bounded by strong gradients which correspond to identified physical phenomena.

Before $-390\,m$ from the shock front the medium is expected to be in equilibrium. At about $-390\,m$, we enter the Lyman-continuum precursor, the RND of electrons, α, increases because of photoionizations. At $x \simeq -1\,m$, α reaches a plateau, because the distance to the shock front becomes much smaller than the mean free path of the Lyman-continuum photons. The Lyman-α precursor, computed in the framework of our ZED approximation (see Sect. 2), begins at about $x \simeq -1\,cm$, where the RND of excited H-atoms (β) rises. The shock front (treated as a discontinuity in our model) is reached at the abscissa $x = 0$ which cannot be displayed with the logarithmic scale used Fig. 1.

After the shock front we enter the two-fluid region (Fig. 2). Before $x \simeq 10^{-3}\,m$ all RNDs but β keep a constant value; in this small region the lyman-α radiation reaches a local equilibrium value related to the local value of β. After $x \simeq 10^{-3}\,m$, the H_2-molecules are broken by collisions and the corresponding RND δ decreases; this leads to an increase of the RNDs of both the ground state ϵ and the excited H-atom β. At about $x \simeq 1\,m$, all the molecules have been destroyed and several processes occur almost simultaneously, leading to the various gradients in RNDs at about $x \simeq 10\,m$.

Close to $x \simeq 10\,m$, there is an important transition region between the end of the two-fluid region and to the beginning of the Lyman-continuum recombination zone.

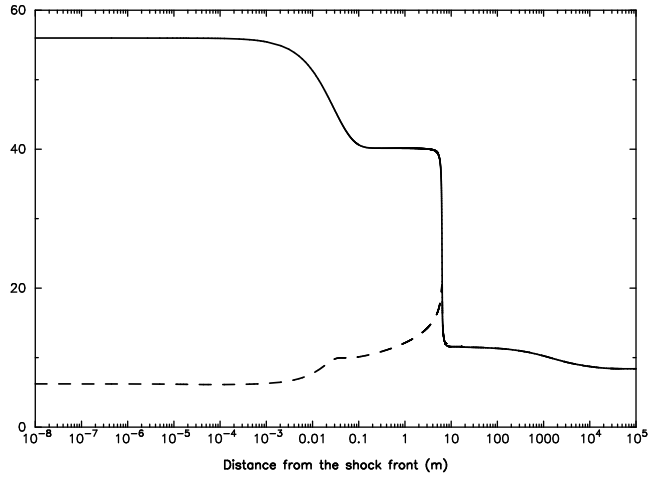

Fig. 4. b Temperature of heavy particles (solid curve) and of electons (dashed curve) versus distance from the shock front in unit of 1000 K.

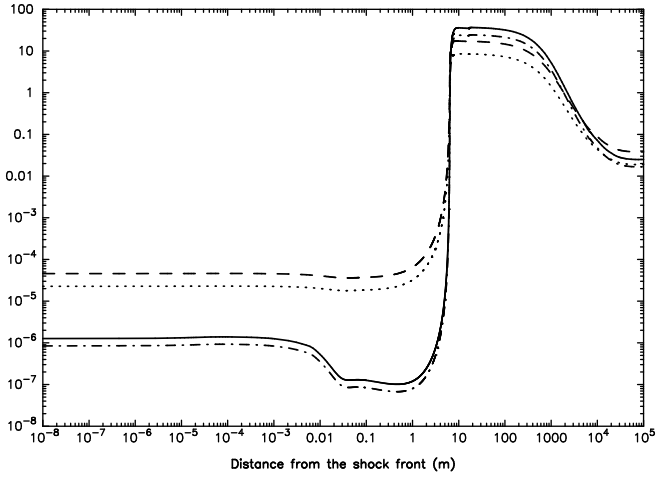

Fig. 4. c Reaction rates versus distance from the shock front throughout the wake in s^{-1}, $C_{c1}\alpha$ (solid curve), $R_{c1}\alpha$ (dashed curve), $C_{c2}\alpha$ (dashed-dotted curve) and $R_{c2}\alpha$ (dotted curve).

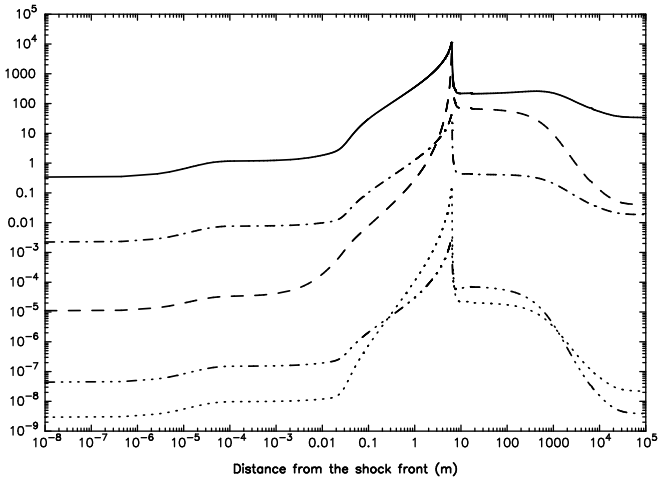

Fig. 4. d Reaction rates versus distance from the shock front throughout the wake in s^{-1}, $C_{21}\beta$ (solid curve), $C_{2c}\beta$ (dashed curve), $R_{2c}\beta$ (dashed-dotted curve), $R^{\alpha}_{2c}\beta$ (dotted curve) and $R^{L}_{2c}\beta$ (dash-three dot curve).

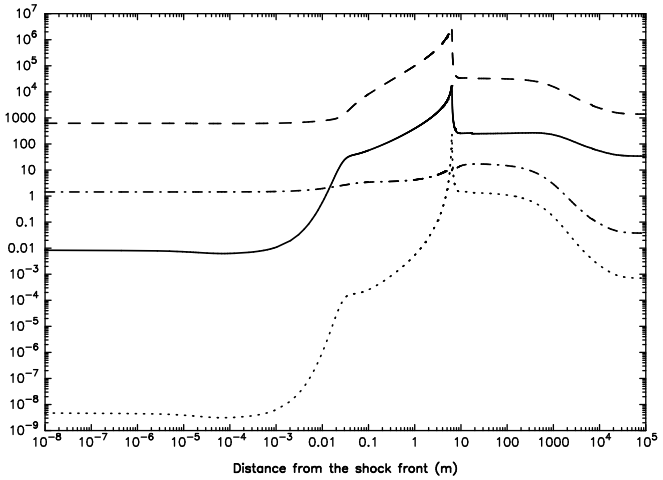

Fig. 4. e Reaction rates versus distance from the shock front throughout the wake in s^{-1}, $C_{12}\epsilon$ (solid curve), $R_{12}\epsilon$ (dashed curve), $R_{1c}\epsilon$ (dashed-dotted curve) and $C_{1c}\epsilon$ (dotted curve).

An important result is that the velocity of the flow (in the frame of the front) falls down to $0.1\,u_0$ in the transition region near $x \simeq 10\,m$. Such a deceleration close to the shock front may produces a very high compression ratio which may produce important secondary effects (dust grains).

Before the two-fluid region all RNDs stabilize and keep constant values until $x \simeq 30\,m$. This behaviour is related to two phenomena: the first one is that before $x \simeq 30\,m$ the medium is optically thin to the Balmer continuum photons. Then, for $x < 30\,m$ the Balmer continuum flux does not influence the RNDs. The second one is that the medium becomes optically thick to the Lyman continum photons, consequently the RNDs tend to reach their local equilibrium values. When the optical thickness in Balmer continuum becomes large enough (after $x \simeq 30\,m$) the system evolves again. If the Balmer continuum flux was not emitted by the gas itself, the system would not show further evolution.

Beyond $x \simeq 30\,m$ we enter an extended region dominated by the recombinations as indicated by the evolution of the RNDs. In the sequel, we shall call this region the Balmer recombination zone. Indeed, the production of both Lyman continuum photons and Balmer continuum photons starts at the same time just after the two-fluid region but the production of Balmer continuum photons becomes significant (with significant changes in the net flux) beyond $x \simeq 30\,m$.

In the Balmer recombination zone, as in the Lyman continuum recombination zone, the velocity decreases and, due to the mass conservation, the density increases. The density at the end of the Balmer recombination zone is about twenty times greater

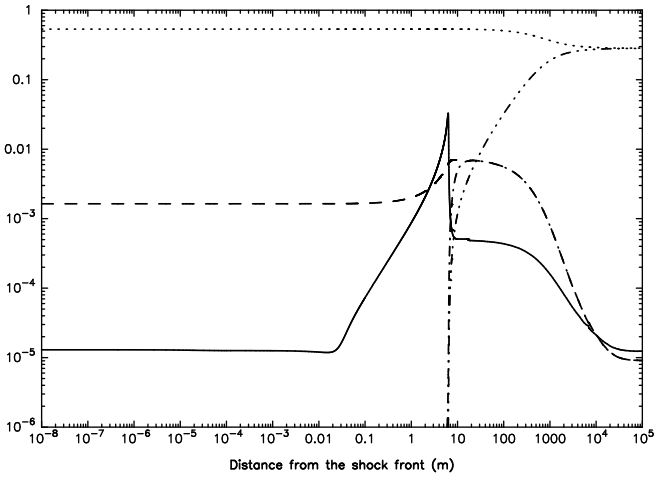

Fig. 4. f Radiative fluxes versus distance from the shock front, in units of F_n, through the wake, F_α (solid curve), $-F_L^-$ (dashed curve), F_L^+ (dashed-dotted curve), $-F_B^-$ (dotted curve) and F_B^+ (dash-three dot curve).

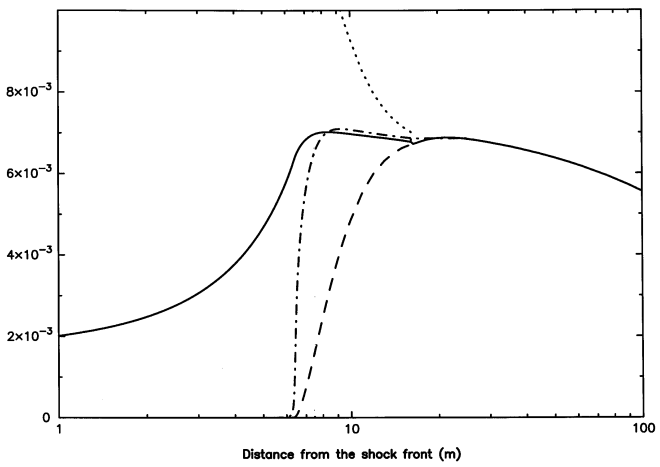

Fig. 4. g Lyman continum flux versus distance from the shock front in units of F_n. Detail of the branching of $-F_L^-$ (solid curve) on F_L^+ (dashed curve). The assymptotic approximations F_0^L (dashed dotted curve) and F_a^L (dotted curve) show that the determination of the Lyman continum flux is self-consistent.

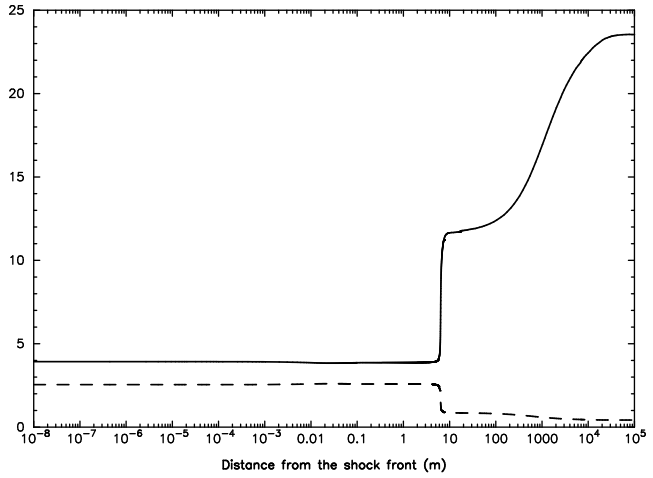

Fig. 4. h ρ/ρ_0 (solid curve) and $10\,u/u_0$ (dashed curve) versus distance from the shock front.

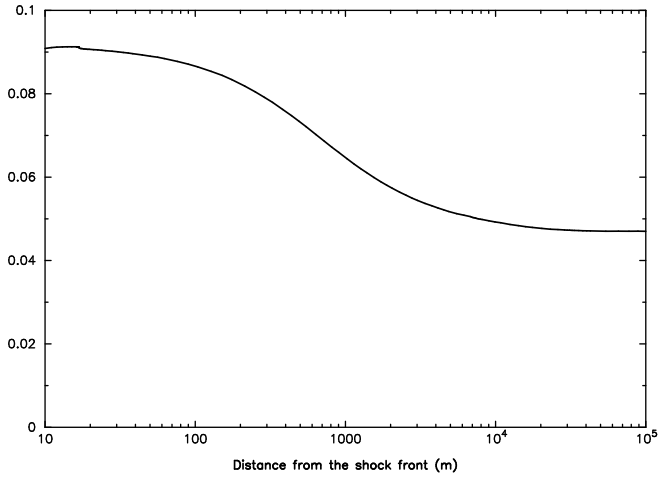

Fig. 4. i Function f (Eq. 3) versus distance from the shock front in the Balmer recombination zone.

than the initial density. Such a variation indicates with a high probability that radiative shock waves do not cross the medium in which they propagate without producing strong perturbations.

The end of the Balmer recombination zone is located at about $x \simeq 10^5\,m$ which is much larger than all wake sizes considered in papers in this series. At this distance from the shock front the energy lost by the structure due to the Balmer continuum radiation can be estimated (see Sect. 6.5) about 75 %.

5. The new model: detailed analysis

Here we discuss the physical phenomena at work in all the identified substructures of the model.

5.1. The precursor

Fig. 2 and Fig. 3 show the precursor structure through the RNDs and the fluxes respectively. The temperature and density have not been displayed because there is no appreciable change for these variables in the precursor.

The precursor is mainly structured by two processes: the photo-ionization of H-atoms and the photo-dissociation of H_2-molecules. The other processes have a negligible influence in our range of parameters. Thus, the structure of the precursor is affected by molecules only through photo-dissociation. Since the photo-dissociation of one H_2-molecule leads to two ground state H-atoms, the effect of H_2-molecule is to delay photo-

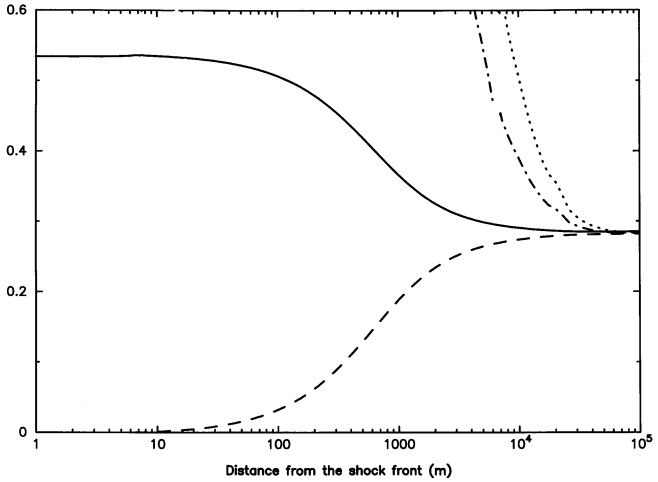

Fig. 4. j Balmer continum flux versus distance from the shock front in unit of F_n. Details of the recombination zone, $-F_B^-$ (solid curve), F_B^+ (dashed curve), F_0^B (dashed dotted curve) and F_a^B (dotted curve).

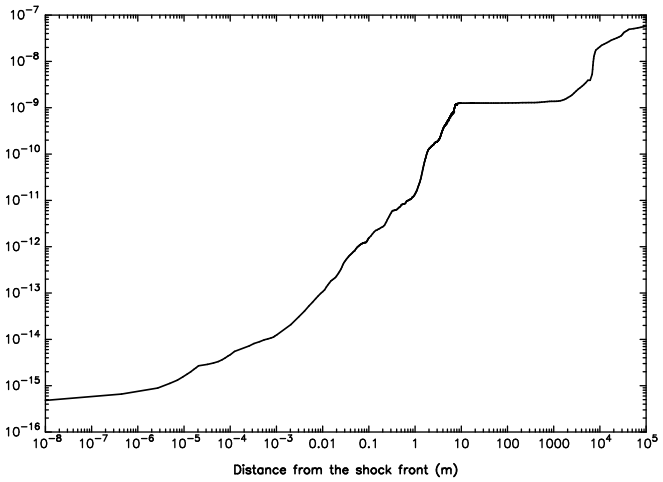

Fig. 5. Cumulative error versus distance from the shock front on the conservation of the total number of protons through the wake.

ionization, and subsequently to increases the precursor size: the number of Lyman continuum photons used to reach some given ionization degree at the shock front is greater when molecules are present.

No excited atoms are assumed present before $x \simeq -1\,cm$, this is a consequence of the ZED approximation. Indeed, as explained in Paper VI, the aim of the ZED approximation is to give an estimate of the amount of excited H-atoms close to the shock front. In particular, the ZED approximation does not take directly into account scattering of the Lyman-α photons. In fact, there is also an extended Lyman-α precursor before $x \simeq -1\,cm$. Inside it, some Lyman-α photons move owing to the excitation/de-excitation process: this leads to what we call a "photon soup". This "photon soup" and the corresponding excited atoms flow with the gas towards the wake. The RND β in what we can call the "optically thick Lyman-α precursor" is, at most, of the same order as the "optically thin Lyman-α precursor" (after $x \simeq -1\,cm$) because, first, there is no source of Lyman-α photons in the precursor other than the Lyman-α photons coming from the wake and, secondly, there is no source of excited atoms in the precursor other than the photo-excitation of H-atoms by the Lyman-α photons. Thus, the calculation of the "optically thick Lyman-α precursor" (which, as explained in Paper VI, is certainly a huge work) is omitted in the framework of the ZED approximation.

Finally the Lyman-α precursor that appears beyond $x \simeq -1\,cm$ is the optically thin Lyman-α precursor in which the photo-excitation due to photons coming directly from the wake increases the RND β.

As explained in Sect. 7, even if the estimate of the amount of excited atoms close to the shock front is poor, this has certainly no significant influence on the whole structure.

5.2. The two-fluid region

The first phenomenon occuring in the two-fluid region is concerned by the Lyman-α radiation.

Distances from the shock front smaller than $x \simeq 10^{-4}\,m$, are smaller than both the mean free path of the Lyman-α photons l_α and the de-excitation length l^* resulting from the de-excitation time at the velocity of the fluid. There, the Lyman-α radiation (Fig. 4a) is neither in radiative equilibrium nor in equilibrium with matter, Eq. (B22) is a truly differential equation.

Beyond $l^* \simeq 10^{-4}\,m$ de-excitation occurs almost locally , F_0^α gets close to F_α and Eq. (B22) degenerates into a non-differential equation, though the medium remains optically thin (as long as $x < l_\alpha$). There is a "photon soup" like that invoked for the precursor in the previous section .

Finally, the Lyman-α photons become trapped in the gas. It follows that the evolution of the RND of excited atoms is governed by radiative equilibrium. More precisely the degeneracy of Eq. (B22) implies that of Eq (B15) because $R_{21}\,\beta$ and $R_{12}\,\epsilon$ are the leading terms of Eq. (B15) and become very close to each other when F_α reaches its local equilibrium value. Thus, there is a "rigid coupling" between β and ϵ.

The collisional dissociation of H_2-molecules (which, in the wake, dominates the photo-dissociation) starts beyond a few $10^{-4}\,m$ (Fig. 2). This produces mainly two correlated effects. The first one is, of course, an increase of the RND of H-atoms. The second is a decrease of the temperature of heavy particles T_h (Fig. 4b): the thermal energy is used to break molecules.

The increase of the RND of H-atoms is followed both by an increase of the RND of excited atoms (because of the above discussed coupling) and by an increase of the RND of electrons (due to photo-ionizations). Then, the rate of collisions between electrons and heavy particles increases, which subsequently increases the temperature of electrons. This, in turn, raises the collisional rates (except the recombination rates).

When almost all molecules are destroyed, ϵ and T_h reach a plateau, located between $x \simeq 10^{-3}\,m$ and $x \simeq 5\,m$ (Figs. 2 and 4b), throughout which the ionization and the correlated

increase of the electronic temperature are the important phenomena.

The increase of α, which at the end of the two-fluid region leads to the sometime called "ionization burst", depends on several processes (Figs. 4c-e). The photo-ionisation from ground state H-atoms dominates the other ionization processes before $1\,m$. Between $1\,m$ and $4\,m$ the photo-ionization from the excited level becomes dominant. Finally, after $4\,m$ the main source of electrons becomes the collisionnal ionization from the excited level.

It is worth noting that, between $1\,m$ and $5\,m$, the coupling between ϵ and β plays an important role: it allows efficiency for the locally most efficient ionization processes, the photo-ionization of excited atoms before $4\,m$, the collisional ionization of excited atoms after $4\,m$, governing the most abundant species, the ground state atoms. In other words, the ground state atoms, which are much more abundant than any other species between $1\,m$ and $5\,m$, fill a reservoir; owing to the coupling between ϵ and β, the RND of excited atoms β is kept at its local value due to an "instantaneous" counterbalancing of ionization. Finally, the presence of excited atoms reduces the length through which the thermalization between electrons and heavy particles is achieved.

At $x \simeq 5\,m$ the RND ϵ becomes sensitive to the various ionization processes, and decreases through a transition region.

5.3. The transition region

Altough the two-fluid region and the Lyman-continuum region can be considered as separated for most of our analysis, there is no acute separation between them and, in fact, these two regions overlap at $x = 6\,m$. Inside the intermediate region some rather violent phenomena occur. For instance, the temperature of heavy particles falls down from about $3.5\,10^4\,K$ to about $1.5\,10^4\,K$ over a distance of $30\,cm$. Indeed, all the variables but the Balmer continuum fluxes (F_B^- and F_B^+) exhibit also strong variations in this region.

Let us look especially to the velocity u: this variable is particularly crucial for the interpretation of observed spectra. Besides, the other variables depend highly on the density, which is directly related to it.

The equations for conservation of mass, momentum and energy can be combined to give

$$u = \gamma_h \frac{Q}{K}\left(1 - \left(1 - f\right)^{\frac{1}{2}}\right) \qquad (1)$$

where

$$f \equiv -2\,\frac{\gamma_h - 1}{\gamma_h^2}\left(\frac{K}{Q}\right)^2$$

$$\left(\frac{3}{2}\,\frac{k\,T_e}{m}\,\alpha + \frac{k\,T_H}{m}\,\alpha + \frac{3}{4}\,\frac{k\,T_H}{m}\,\beta + \frac{k\,T_D}{2\,m}\,(1-\delta) + \frac{F}{K} - E\right) \qquad (2)$$

From the equation for conservation of energy (B3), $f \geq 0$, and since $u > 0$ then $f > 0$. The term under the square root of Eq. (1) must be positive thus, $f \leq 1$; in addition, for $f = 1$, u is maximum and one can verify *a posteriori* that this maximun is never reached inside the wake. Finally, $0 < f < 1$.

Eq. (2) can be simplified using the following inequalities (which hold everywhere in the wake):

$$T_e \ll T_H$$

$$\left|F_L\right| \ll \left|F_B\right|$$

$$\beta \ll \alpha$$

In addition, almost all molecules have been destroyed before the transition region so that, in the transition region Eq. (2) reduces to

$$f = 2\,\frac{\gamma_h - 1}{\gamma_h^2}\left(\frac{K}{Q}\right)^2\left(E - \frac{k\,T_D}{2\,m} - \frac{k\,T_H}{m}\,\alpha - \frac{F_B}{K}\right) \qquad (3)$$

Since F_B is practically constant throughout the transition region (Fig. 4f) this expression shows that the variations of u are due to the ionization of the gas (characterized by α); the ionization mechanism is that described in Sect. 6.2.

To conclude, the strong gradients which appear in the transition region are triggered by a mechanism that may be called "self-stimulated ionization" in the sense that an increase of the RND of electrons leads (by different ways) to an increase of the rate of ionization. It is worth noting that excited atoms, though not necessary, strengthen this effect.

5.4. The recombination region: the Lyman continuum dominated zone

Recombinations start within the just discussed transition region (Fig. 4c), and both continua are produced in this region. Here, we first describe that part of this region in which the Lyman continuum is produced, that is before $x \simeq 30\,m$.

There, the integration becomes numerically unstable. This behaviour, which is mainly due to Eq. (B21), has been analysed in Paper III: in the Lyman continuum recombination zone, the system reaches the radiative equilibrium for the Lyman continuum, that is the net radiative flux tends to zero and the photon density reaches a value determined by the local state of the gas: Eq. (B21) degenerates progressively into a non-differential equation. The value of F_L^- must remain close to the local value of F_0^L; this is one of the boundary conditions for Eq. (B21). More precisely, we have $\left(F_L^- - F_0^L\right) \longrightarrow 0$ when $x \longrightarrow +\infty$. This condition is satisfied when the shooting parameters are correctly adjusted, that is when the solution is self-consistent. Roughly speaking, if the value of F_L^- at the shock front (which is the value at the end of the precursor) is not the "true" value (the flux emitted by the wake), then Eq. (B21) does not degenerate at the "right place".

Indeed, our solution is now obtained after many guesses and owing to the improvement of the computational scheme (Sect. 3).

Now, when the model of the H-atom includes only two levels (ground level and continuum) as in Paper III, the degeneracy of Eq. (B21) implies the degeneracy of all the RND equations

(see Paper III for more details). When the first excited level is taken into account, a new RND equation is required and some additional terms appear. The degeneracy of the RND equations observed in the "two-level model" no longer holds, because the additional terms in RND equations are not all negligible compared to the others (Fig. 4c-e), and the coupling produced by the degeneracy of the Eq. (B21), namely $R_{1c}\,\epsilon \simeq R_{c1}\,\alpha$, does not stop the evolution of the system as previously, but it freezes the system for some time: all quantities but fluxes reach a plateau after the transition region.

To understand this behaviour, consider the RND equations (B14-B16): the only non-local term is $R_{c2}\,\beta$, related to the Balmer flux, and as long as this term is small (Figs. 4c-e), the RNDs are determined by the local state of the gas. Now, the thermodynamical variables are in close relation with the velocity. Eqs. (1) to (3) show that the velocity can be changed by a variation of α and/or a variation of the net Balmer flux F_B. While α keeps a "quasi-equilibrium" value function of the local state of the gas, the velocity, and subsequantly the other thermodynamical variables, keep a quasi-constant value until F_B is varied significantly: the gas remains in a quasi-equilibrium state.

The upstream Lyman continuum flux can be switched onto its zero order approximation close to $x = 20\,m$ (Fig. 4g). The optical depth is about 5 and the solution is not significantly perturbed by the switch. Nevertheless, the system of equations is sufficiently sensitive to induce a small numerical step variation (obvious in Fig. 4h). This has no influence on the results.

Finally, at $x \simeq 30\,m$ the variations of the Balmer continuum flux becomes sufficient to modify the velocity and the gas leaves its quasi-equilibrium value.

5.5. The recombination region: the Balmer continuum part

As just mentioned, though the recombinations onto the first excited level start beyond the two-fluid region, the emission of the Balmer continuum photons becomes significant only beyond $x \simeq 30\,m$.

Fig. (4h) shows that the density increases over a large distance (about $10\,km$). As in the transition region, this behaviour can be explained using Eq. 3, the difference is now that the net Balmer flux F_B varies. Fig. 4i displays the function f (Eq. 3), which is decreasing.

Integration is performed up to an optical depth of about 10, at a distance from the shock front of about $100\,km$ (Fig. 4j). The upstream and downstream Balmer fluxes are close to the local approximations (F_0^B and F_a^B), which ensures the self-consistency of the calculations.

Now a new numerical problem appears: if, at the fairly large optical depth reached, the upstream Balmer flux F_B^- is replaced by the local value F_0^B (as usual in the two-stream method) the resulting error affects directly the velocity because it is sensitive to the Balmer continuum net flux (see Eq. 3). The difference with what occurs when switching the Lyman continuum is that now the switch onto F_0^B leads to a stronger discontinuity in the velocity; the problem is that this discontinuity influences the whole system of equations in a non-linear way. In particular the temperature (which depends on u^2) also exhibits a step variation which leads to a more erroneous value of the collisionnal rates and, subsequently, of the RNDs. In any case since this problem appears at a fairly large optical depth, the self-consistency of the solution is preserved.

Finally, consider the energy emitted in the Balmer continuum. This energy escapes from the whole structure. It can be characterized by the ratio

$$\frac{-F_B^-}{\frac{1}{2}\,\rho\,v_0^3}$$

which represents that part of the initial kinetic energy flux which has been transfered into Balmer continuum flux and "lost" by the shock wave. In the present case this quantity is about 75 %. This value is smaller than that found by Narita (1973) for analogous initial values, which was 88 %. This difference is mainly due to the three-body recombination rates which are greater in our work and to the fact that the H_2-molecules are neglected in the Narita's.

6. Some tests concerning the solution

In Sect. 1. we explained that, due to the complexity of the problem, our modelization is not an extensive and highly accurate description of the radiative shock waves which are expected to propagate in some circumstellar media dominated by collisions, but a modelization as consistent as possible, providing information on how such shocks are structured. Here, let us again emphasize that "as consistent as possible" means that all the approximations used in our modelization must all have insofar as possible the same level of accuracy. The difficulty is to check the validity of the approximations made, because the interpretation of observational or experimental data requires models much more accurate than those available at the present time. Nevertheless, it is possible to estimate the sensitivity of the model to approximations which may seem the less robust. This is the purpose of this section.

For clarity the solution presented in Sects 4. and 5. is referred to as $S1$ in this section.

6.1. Influence of the amount of excited H-atoms at the shock front

As already explained the purpose of the ZED approximation is to provide the necessary estimation of the RND β close to the shock front: hereafter we shall denote it β_f . In the ZED approximation, β_f is underestimated because scattering of the Lyman-α photons is omitted. The problem we are looking at is then the rearrangement of the whole structure following a larger value of β_f. The best to do this is to increase the value of σ_{12} up to $10^{-12}\,cm^2$ (which is certainly an overestimation of the true value) in the precursor.

The only differences with $S1$, apart from the artificial reduction of the size of the Lyman-α precursor, are concerned with

Table 1. Comparison of the (shooting) parameters for the solutions obtained with modified three-body recombination rates

	v_s	α_f	$\pi_{B,-\infty}$
	$(km\,s^{-1})$		–
$0.2\,R_3$	41	$1.16\,10^{-3}$	$2.5\,10^{-4}$
$5\,R_3$	–	$7.7\,10^{-4}$	$2.3\,10^{-4}$
R_3	–	$1.0\,10^{-3}$	$2.4\,10^{-4}$

the RND of β and the Lyman-α flux before $x \simeq 10^{-1}\,m$. The rest of the solution with the enhanced β_f is almost identical to $S1$.

6.2. Influence of the rate of three-body recombinations

The result concerning the three-body recombination in Paper VII suggests that this process can play an important role in the radiative relaxation region of the wake. However, as explained (see Sect.2.3.2) the determination of the rate of three-body recombinations raises different problems. In Paper VII, the problem was solved by elaborating a specific approximation sufficient to give informations about the influence of the three-body recombinations in the wake.

However, under the condition of Paper VII, a test of the sensitivity of the model to our approximation concerning R_3 (Appendix C) was impossible because of numerical instabilities in the Lyman continuum zone stopping integration too early, before recombinations have a significant effect.

Now, some simple tests are possible. The calculations performed with values greater or smaller than that used for $S1$ illustrate the sensitivity of the structure to the three-body recombination rates.

Input parameters are compared in Table 1. In the case of the smaller rate (R_3 is decreased by 80%) the variation of α_f is + 15 % and the variation of the Balmer continuum flux is + 5%. In the case of the increased rate (R_3 is increased by 400%) the variation of α_f is $-$ 25 % and the variation of the Balmer continuum flux is $-$ 5%. This values shows that $S1$ is weakly changed by variations of R_3.

Now, when the rate of three-body recombinations increases, the RND of atoms is increased, then the opacity in the continua increases and the net continuum fluxes becomes smaller. This explains the variations of the Balmer flux, those of α_f (which depends directly of F_L^-), and those of the velocity in the Balmer recombination region (since u depends of F_B through Eq. 1). The variation of the RNDs are directly related to the change of R_3. The Lyman-α flux follows the RNDs β and ϵ as explained Sect. 6.2.

Another point is concerned by the parameter η which is the branching ratio between three-body recombinations leading to a ground-state H-atoms and those leading to an excited H-atom. In $S1$, η was set equal to 0.4, a value close to the maximum value of η. This value has been replaced by 0.3, a value close to its minimum value (see Paper VII), without any significant change on the results.

Finally, fairly large variations of the three-body recombination rate R_3 have very moderate effects on our solution. Then, despite the relative inaccuracy of the value of R_3 resulting of the approximation elaborated in Paper VII, it seems that this approximation is reasonable in the framework of our model.

6.3. Modification of the parameter $\tilde{T}_{e,B}$

The sensitivity of the solution to the parameter $\tilde{T}_{e,B}$ may appear only through the processes related to the Balmer continuum (mainly the photoionization of excited H-atoms and the radiative recombinations onto the excited level): increasing $\tilde{T}_{e,B}$ is equivalent to increase the frequency of the mean Balmer photon ν_B and thus to decrease both R_{2c} and R_{c2}. Since both the photoionisation of excited H-atoms and the radiative recombinations on the excited level are not dominant processes, the solution is not affected by a (not so large) modification of $\tilde{T}_{e,B}$.

6.4. Precision of the calculations

Since the RNDs are calculated independently one from the others, Eq. (B6), which expresses the conservation of the total number of protons, provides an estimator of the numerical error made during the calculation. Fig. (5) displays the value of the expression

$$\sum_i \left|\alpha_{c,i} + \beta_{c,i} + \epsilon_{c,i} + \delta_{c,i} - 1\right|$$

where i is the index of the step and the subscript c indicates a computed value. At the end of the calculation this value is below 10^{-7}.

7. Conclusion

The model presented in this paper concludes a new step in the analysis of hypersonic shock waves started in 1983 and based on consistent modelization of the investigated structures. Now, we could model in a self consistent way a thick layer including the radiative Lyman continuum (and Lyman-α) precursor, the hydrodynamic discontinuity, the two fluid non equilibrium post-front zone, the ionization zone, and the two recombination zones where the Lyman continuum and the Balmer continuum are produced. This is the most important layer of the shock front for dynamics (the compression ratio is maximum there) and also thermodynamics (the main thermodynamical features of the shock are certainly governed by the three regions of the spectrum taken into account, and the numerical checks strongly suggests that introducing higher energy levels will probably not change drastically them). Now, physical perturbations produced by the propagation of such waves in circumstellar media must be investigated, but this was out of the scope of this work.

Then, due to the difficulties and the problems encountered and discussed in the previous sections, one should note that obtaining such a model had some coast, expressed in terms of the

approximations which appeared necessary to solve the equations, at our present level of knowledge.

First, it was necessary to limit our field of analysis to "weak enough shocks" (see Sect. 2.2).

Now another limit of the model stems from the mean-photon model. The ZED approximation provides a local status to the photons which is not accurate if there is diffusion in the wings of the Lyman-α line (see Sect. 6.1).

Another problem is concerned by the interaction between Lyman-α photons and molecules, which is ignored in the present work.

The part of the precursor, and the optically thin region following the front, governed by the Lyman-α radiation as described in the model are very small and probably not very much thicker than layers produced by the ignored processes of the front. An improved description of these layers is necessary for a more quantitative analysis.

An important observable feature of strong shocks is the H_α line, which is also sensitive to the overall structure through the population of the first excited level of the hydrogen atoms. Of course, the model cannot account for this line, because of the lack of energy levels in our hydrogen atom. However, it allows to expect that this line will be produced in a fairly thick region including several substructures of the post-front region, so that one should not derive too precise conclusions from observations interpreted using classical models of the H_α line formation under equilibrium conditions.

A last, but not least problem remains: the models emphasize the importance of the role of the three-body recombinations in the wake, but at this time, the actual effects of this process is still not well known from a pure physical point of view, under the conditions which are those (strongly out of equilibrium) of the shock wake.

To conclude, the presented model is a good tool to estimate with some confidence good orders of magnitude for the effects produced by the various involved processes, and also to emphasize the strong not negligible effects due to assumptions classical for media at equilibrium but excessive for media out of equilibrium. It also confims the non local properties of the shock layers, suggesting that the problem is still huger if time dependence is introduced: then not only influence of various regions but also the past history of these regions must be taken into account for estimating the balance at each point.

Appendix A: microscopic processes

The reactions under consideration and their corresponding reaction rates are listed below for the precursor and the wake. The origin of the reaction rates was listed in Paper VII.The only modification is concerned by the photo-ionization cross-section from the ground level which is now given by the more accurate value (Zel'Dovich and Raiser, 1966)

$$\sigma_{1c} = 6.34\,10^{-18}\,(\frac{\nu_{L,0}}{\nu_L})^{2.67}$$

where $\nu_{l,0}$ is the ionization frequency of the ground state hydrogen atom.

A.1. Microscopic processes considered in the precursor

H_2	+	$h\nu_{id}$	$\longrightarrow$	H	+	H			, R_{id}
H^*	+	e	$\longrightarrow$	H^+	+	e	+	e	, C_{2c}
H	+	e	$\longrightarrow$	H^*	+	e			, C_{12}
H^*	+	e	$\longrightarrow$	H	+	e			, C_{21}
H	+	e	$\longrightarrow$	H^+	+	e	+	e	, C_{1c}
H	+	$h\bar{\nu}_L$	$\longrightarrow$	H^+	+	e			, R_{1c}
H	+	$h\bar{\nu}_\alpha$	$\longrightarrow$	H^*					, R_{12}
H^*	+	$h\bar{\nu}_B$	$\longrightarrow$	H^+	+	e			, R_{2c}
H^*	+	$h\bar{\nu}_\alpha$	$\longrightarrow$	H^+	+	e			, R^α_{2c}
H^*	+	$h\bar{\nu}_L$	$\longrightarrow$	H^+	+	e			, R^L_{2c}

A.2. Microscopic processes considered in the wake

H_2	+	H_2	$\longrightarrow$	$2\,H$	+	H_2	, C_{1d}
H_2	+	H	$\longrightarrow$	$3\,H$			, C_{2d}
H^*	+	e	$\longleftrightarrow$	H^+	+	$2\,e$	, $C_{2c}; C_{c2}$
H	+	e	$\longleftrightarrow$	H^+	+	$2\,e$	, $C_{1c}; C_{c1}$
H	+	e	$\longleftrightarrow$	H^*	+	e	, $C_{12}; C_{21}$
H	+	$h\bar{\nu}_L$	$\longleftrightarrow$	H^+	+	e	, $R_{1c}; R_{c1}$
H^*	+	$h\bar{\nu}_B$	$\longleftrightarrow$	H^+	+	e	, $R_{2c}; R_{c2}$
H	+	$h\bar{\nu}_\alpha$	$\longleftrightarrow$	H^*			, $R_{12}; R_{21}$
H^*	+	$h\bar{\nu}_\alpha$	$\longrightarrow$	H^+	+	e	, R^α_{2c}
H^*	+	$h\bar{\nu}_L$	$\longrightarrow$	H^+	+	e	, R^L_{2c}

Appendix B: equations of the model

B.1. The conservation equations

Conservation of mass, momentum and energy are expressed as

$$K \equiv \rho\, u \tag{B1}$$

$$Q \equiv \rho\, u^2 + p \tag{B2}$$

$$E \equiv \frac{1}{2}\,u^2 + \sum_i \theta_i\, e_i + \sum_i \theta_i\, \frac{p_i}{\rho_i} + \frac{k}{m_H} \left(\left(\alpha + \frac{3}{4}\,\beta\right) T_H + \frac{1}{2}\left(1 - \delta\right) T_d\right) + \frac{F}{K} \tag{B3}$$

with

$$\theta_i \equiv \rho_i/\rho$$

$$e_i = \frac{1}{\gamma_i - 1}\,\frac{p_i}{\rho_i} \tag{B4}$$

and where K, Q, E are constants, F is the net radiative flux.

The electric neutrality reads

$$\alpha \equiv \frac{n_e}{n} = \frac{n_{H^+}}{n}. \tag{B5}$$

The conservation equation for the total number of protons reads

$$\epsilon + \beta + \alpha + \delta = 1 \tag{B6}$$

These equations hold anywhere throughout the shock structure.

B.2. The equations describing the precursor

The equations for the relative number density read

$$\frac{d\epsilon}{dt} = \Big[R_{id}\,Y\big(\bar{\nu}_L - \nu_{id}\big)\Big]\,\delta + C_{21}\,\beta - \Big[C_{12} + R_{1c} + C_{1c} + R_{12}\Big]\,\epsilon \quad \text{(B7)}$$

$$\frac{d\beta}{dt} = \Big[C_{12} + R_{12}\Big]\,\epsilon - \Big[C_{21} + C_{2c} + R_{21} + R_{2c} + R^{\alpha}_{2c} + R^{L}_{2c}\Big]\,\beta \quad \text{(B8)}$$

$$\frac{d\alpha}{dt} = \Big[C_{2c} + R_{2c} + R^{\alpha}_{2c} + R^{L}_{2c}\Big]\,\beta + \Big[C_{1c} + R_{1c}\Big]\,\epsilon \quad \text{(B9)}$$

$$\frac{d\delta}{dt} = -\Big[R_{id}\,Y\big(\bar{\nu}_L - \nu_{id}\big)\Big]\,\delta \quad \text{(B10)}$$

The equations for the number density of photons read

$$\frac{u}{K}\,\frac{d}{dx}\big(\pi_i\,\rho\,c\big) = s_i \quad \text{(B11)}$$

with

$$s_L = \frac{1}{2}\,\kappa\,R_{id}\,Y\big(\bar{\nu}_L - \nu_i\big)\,\delta + R_{1c}\,\epsilon + R^{L}_{2c}\,\beta$$

$$s_B = R_{2c}\,\beta$$

$$s_\alpha = R_{12}\,\epsilon + R^{\alpha}_{2c}\,\beta$$

The equation for the density reads

$$\frac{d\rho}{dx} = g_0 + g_1\,\frac{d\alpha}{dx} + g_2\,\frac{d\beta}{dx} + g_3\,\frac{d\epsilon}{dx} \quad \text{(B12)}$$

The equation for the temperature reads

$$\frac{dT}{dx} = f_0 + f_1\,\frac{d\alpha}{dx} + f_2\,\frac{d\beta}{dx} + f_3\,\frac{d\epsilon}{dx} + f_4\,\frac{d\rho}{dx} \quad \text{(B13)}$$

The functions f_i and g_i are detailled in (Huguet et al., 1992).

B.3. The equations describing the wake

B.3.1. The equations for the relative number densities

$$u\,\frac{d\epsilon}{dx} = -\Big[C_{12} + R_{12} + R_{1c} + C_{1c}\Big]\,\epsilon + \Big[C_{c1} + R_{c1}\Big]\,\alpha + \Big[C_{21} + R_{21}\Big]\,\beta + \Big[\frac{1}{2}\,C_{1d} + C_{2d}\Big]\,\delta \quad \text{(B14)}$$

$$u\,\frac{d\beta}{dx} = \Big[C_{12} + R_{12}\Big]\,\epsilon - \Big[C_{21} + R_{21} + C_{2c} + R_{2c} + R^{\alpha}_{2c} + R^{L}_{2c}\Big]\,\beta + \Big[C_{c2} + R_{c2}\Big]\,\alpha \quad \text{(B15)}$$

$$u\,\frac{d\alpha}{dx} = \Big[C_{2c} + R_{2c} + R^{\alpha}_{2c} + R^{L}_{2c}\Big]\,\beta + \Big[C_{1c} + R_{1c}\Big]\,\epsilon - \Big[C_{c1} + R_{c1} + C_{c2} + R_{c2}\Big]\,\alpha \quad \text{(B16)}$$

$$u\,\frac{d\delta}{dx} = -\Big[\frac{1}{2}\,C_{1d} + C_{2d}\Big]\,\delta \quad \text{(B17)}$$

B.3.2. The equations of thermodynamics and hydrodynamics in the two-fluids region

The equation of elecronic temperature reads

$$\frac{dT_e}{dx} = f_{e,0} + f_{e,1}\,\frac{d\alpha}{dx} + f_{e,2}\,\frac{d\beta}{dx} + f_{e,3}\,\frac{d\rho}{dx} + f_{e,4}\,\frac{dF}{dx} \quad \text{(B18)}$$

The functions $f_{e,i}$ are detailled in PaperVII.

The equation for the temperature of heavy particles reads

$$T_h = \frac{2}{2-\delta}\,\frac{m_H}{k}\left(-u^2\big(\alpha_i,T_e\big) + \frac{Q}{K}\,u\big(\alpha_i,T_e\big) - \frac{k}{m_H}\,\alpha\,T_e\right) \quad \text{(B19)}$$

Finally, the derivative of the density is calculated by using an Euler method.

B.3.3. The equations of the one fluid region

After thermalization, the temperature T of the flow is obtained from Eq. (B19) setting $T = T_h = T_e$, which leads to

$$T = \frac{m_H}{k}\left(-u^2\big(\alpha_i,T\big) + \frac{Q}{K}\,u\big(\alpha_i,T\big)\right) \Big/ \left(1 - \frac{\delta}{2} + \alpha\right) \quad \text{(B20)}$$

We obtain all other gasdynamic quantities of the model using the conservation equations.

B.3.4. The transfer equations

The transfer equations read

$$\frac{dF_i^{\,-}}{dx} = \frac{1}{2}\,j_i + \sqrt{3}\,\kappa_i\,F_i^{-} \quad \text{(B21)}$$

$$\frac{dF_i^{\,+}}{dx} = \frac{1}{2}\,j_i - \sqrt{3}\,\kappa_i\,F_i^{+} \quad \text{(B22)}$$

where the subscript i denotes the radiation considered, F_i^+ and F_i^- are the algebraic values of the fluxes propagating towards increasing x (downstream) and decreasing x (upstream) respectively; j_i and κ_i are the emissivity and the opacity.

$$j_L = h\nu_L\,R_{c1}\,n\,\alpha \quad \text{(B23)}$$

$$j_B = h\nu_B\,R_{c2}\,n\,\alpha \quad \text{(B24)}$$

$$j_\alpha = h\nu_\alpha\,R_{21}\,n\,\beta \quad \text{(B25)}$$

$$\kappa_L = \sigma_{1c}\,n\,\epsilon + \sigma_{2c}\,n\,\beta \quad \text{(B26)}$$

$$\kappa_B = \sigma_{2c}\,n\,\beta \quad \text{(B27)}$$

$$\kappa_\alpha = \sigma_{12}\,n\,\epsilon + \sigma^{\alpha}_{2c}\,n\,\beta \quad \text{(B28)}$$

The Lyman-α net flux is taken equal to zero at the shock front. Consequently $F^+_\alpha = -F^-_\alpha$ at the front but also everywhere and only one of the transfer equations is necessary. We take Eq. (B22) in which we replace F^+_α by the notation F_α ($F_\alpha > 0$).

Appendix C: notations

C_{mn}	Collisional transition rate from the level m to the level n per second
e	Electron charge
E	Total energy per unit of mass
e_i	Internal energy per unit of mass
E_n	Energy of the level n of the hydrogen atom
E'	Binding energy when the separation between two bound levels is equal to kT_e
F	Total net radiative flux: $F \equiv \sum_i F_i$
F_i^+	Upstream flux for the radiation i
F_i^-	Downstream flux for the radiation i
F_0^i	Local value of the flux of the radiation i
F_a^i	First order approximation of the flux of the radiation i
F_i	Net flux of the radiation i: $F_i \equiv F_i^+ + F_i^-$
F_n	Energy flux necessary to ionize completly all the hydrogen atoms crossing the shock front per unit of time ($F_n \equiv \left(k\,T_H/m_H\right)\, rho_{-\infty}\, u_{-\infty}$)
f_i	Functions appearing in the equation of temperature of the precursor
$f_{e,i}$	Functions appearing in the equation of electronic temperature
$f_{h,i}$	Functions appearing in the equation of temperature for heavy particles
g_i	Functions appearing in the equation of density of the precursor
h	Planck constant
j_i	Emisivity corresponding to the radiation i
K	Constant corresponding to the conservation of the mass (ρu)
k	Boltzmann constant
l_α	Mean free path of the Lyman-α photons
l^*	Length necessary to de-excite an hydrogen atom entrained by the fluid
m_x	Mass of the particles of species x
n	Number density
n_x	Number density of the particles of species x
p	Gas pressure
p_x	Partial pressure of the gas of particles x
Q	Constant corresponding to the conservation of the momentum ($\rho u^2 + p$)
R_{mn}^l	Radiative transition rate from level m to level n due to the radiation l (s^{-1})
R_3	Reaction rate for the three-body recombination process
T	Temperature
T_H	Temperature corresponding to the binding energy of the hydrogen atom
T_x	Temperature of particles x
$T_{e,L}$	Temperature corresponding to the Lyman continuum mean photon
$T_{e,B}$	Temperature corresponding to the Balmer continuum mean photon
u	Gas velocity relative to the shock front
v_s	Velocity of the shock front
x	Physical space coordinate
α	Electron relative number density (RND) normalized to n
β	Excited atom relative number density (RND) normalized to n
γ_x	Ratio of specific heat of particles x
δ	Molecule relative number density (RND) normalized to n
ϵ	Ground level atom relative number density (RND) normalized to n
ϵ^+	Ionized atom relative number density (RND) normalized to n
η	Branching ratio to distinguish three-body recombinations leading to a first excited atom from those leading to a ground state atom (see Paper VII).
κ	Correction factor for the two-step photodissociation
κ_i	Opacity for the radiation i
μ	Branching ratio for the two-step photodissociation
ν_i	Frequency of the mean photon for the radiation i
ρ	Mass density (gcm^{-3})
ρ_x	Mass density of the particles x
σ_{ij}^k	Cross-section for a radiative transition betwwen the levels i and j due to or leading to a radiation k

References

Bates D.R., Kingston A.E., McWhirter R.W.P., 1962 PASP A267, 297
Bates D.R., Kingston A.E., McWhirter R.W.P., 1962 PASP A270, 155
Gillet D., Lafon J-P.J., 1983 A&A 128, 53
Gillet D., Lafon J-P.J., 1984 A&A 139, 401
Gillet D., Lafon J-P.J., David P., 1989 A&A 220, 185
Hinnov E.,Hirschberg J.G. , 1962 Phys. Rev. 125, 795
Huguet E., Lafon J-P.J., Gillet D., 1992 A&A 255, 233
Huguet E., Lafon J-P.J., Gillet D., 1994 A&A 290, 510
Huguet E., Lafon J-P.J., Gillet D., 1994 A&A 290, 518
Lafon J-P.J., 1995 Prospect for circumstellear physics. Observations and models. in "Science with the V.L.T.", proc. E.S.O. workshop Garching Germany, 28 jun - 1 july 1994; J.R. Walsh, I.J. Danziger Eds., Springer 1995, p 119
Lafon J-P.J., Berruyer N., 1991 A&AR 2, 249
Narita S., 1973, Prog. Theor. Phys. 49, 1911
Sherman M.P., 1968 J. Quant. Spectrosc. Radiat. Transfer 7, 89
Zel'Dovich Ya.B., Raiser Yu.P., 1966, Physics of shock waves and high-temperature hydrodynamic phenomena Vol 1, Academic Press

This article was processed by the author using Springer-Verlag LaTeX A&A style file *L-AA* version 3.